**ORIGINAL ARTICLE**

# Comparative synthesis of ZrO$_2$ nanoparticles by green and co-precipitation methods: The effect of template on structure

*Hana Aminipoya, Azar Bagheri Ghomi[*], Ali Niazi*

*Department of Chemistry, Central Tehran Branch, Islamic Azad University, Tehran, Iran*

**Abstract**

It was shown that the structure and particle size of zirconia nanoparticles has been controlled through the homogeneous precipitation process by using templates. Hexamine as the template led to ZrO$_2$ nanoparticles with tetragonal structure, whereas coffee extract favored monoclinic structures. Field Emission Scanning electron microscopy (FeSEM), Transmission electron microscopy (TEM) measurements, Infrared and Raman analysis were used to view how the structure may possibly affect their spectrum characteristic. Using these pure m- and t-ZrO$_2$ phases as catalyst, were studied photocatalytic degradation of ciprofloxacin (CIP). Higher degradation efficiency (50%) of the drug was observed at pH5.5 after 15 min using t-ZrO$_2$ phase.

**Keywords:** *FT-IR; Monoclinic; Raman Spectroscopy; TEM; Tetragonal; ZrO$_2$.*

## INTRODUCTION

The nano sized ZrO$_2$ is very interesting and valuable material for its fundamental and application based properties. ZrO$_2$, because of its surface characteristics with acid-base properties and redox functions, has been used as a catalyst in many reactions. The type of zirconia crystalline phase (monoclinic and tetragonal) affects the selectivity and activity of the catalyst [1-4]. For acid-catalyzed *n*-alkane isomerization, sulfated t-ZrO$_2$ was found to be 2-5 times more active than sulfated m- ZrO$_2$. Monoclinic ZrO$_2$ is important for catalysis, [4] gate dielectrics,[5] and bioactive coatings on bone implants, [6] while tetragonal and cubic ZrO$_2$ are promising candidates for fuel cell electrolytes, [7] oxygen sensors, [8] and phase-transformation-toughened structural materials [9].

The differences in their catalytic performance clearly indicate the importance of pure m- and t-ZrO$_2$ synthesis. For this reason, many efforts have been made to synthesize them. m-ZrO$_2$ is

frequently prepared via the hydrolysis of zirconyl chloride under reflux or hydrothermal conditions [10,11]. The synthesis of undoped t-ZrO$_2$ has been achieved generally by using zirconium alkoxides as precursors via sol-gel, solvothermal, and spray pyrolysis methods [12–19]. Also, the bean of coffee was earlier reported to contain good levels of phenolic compounds [20]. However, many pure m- and t-ZrO$_2$ synthesis methods are complex and require strict control of reaction parameters such as temperature, pressure and pH or the use of relatively expensive and toxic zirconium alkoxides. In continuation of studies done in this area we have focused on the design and preparation of ZrO$_2$ NPs as an efficient heterogeneous catalyst [21-23]. For example, researchers reported synthesis of T- ZrO$_2$ nanoparticles for photocatalytic and antimicrobial activity [23, 24]. Therefore, we made an attempt to study the photocatalytic activity of pure synthesized nanoparticles. In this context, simple, easy synthesis routes are highly desired, especially for the practical applications of ZrO$_2$ nanoparticles of pure phases. ZrO$_2$ nanostructures were

* Corresponding Author Email: *azar.bagheri@iauctb.ac.ir*

successfully synthesized starting from zirconium chloride in aqueous solution through two different approaches including green synthesis using bean of coffee and a simple Co-precipitation method. Also, in this study, the effect of synthesis method on morphology and physical properties of the resulting products is investigated.

**EXPERIMENTAL**

Phase identification of the fabricated sample was carried out by a Holland Philips X-ray diffraction CuKα (λ=1.5417 Å) in the radiation range of 20°–80°. A Field emission scanning electron micrograph (FeSEM) of a Holland Philips XL30 microscope was used to observe the morphology and elemental analysis of the sample. Transmission electron microscopy (TEM) analysis was performed on a Zeiss-EM10C-100 KV. The Raman spectrum was recorded in the spectral range 200–1400 cm$^{-1}$ using Almega Thermo Nicolet Raman spectrometer. The presence of surface functional groups in the prepared samples was analyzed by FTIR spectrum recorded using Perkin Elmer FTIR spectrometer. Spectrophotometric measurements were conducted using an UV-vis Shimadzu 2101 spectrophotometer equipped with a Acermate 486 SX/25D computer and thermostically matched 10-mm quartz cells.

To prepare the coffee extract, 400 mg of coffee powder (coffee powder 99%) was dissolved in 50 mL of water. $ZrO_2$ nanoparticles were synthesized by adding the corresponding extracts to 0.1 M aqueous zirconium chloride solution in a 1 : 1 volume ratio at room temperature by constant stirring for 24 h. $ZrO_2$ was obtained by centrifugation and drying of precipitate at room temperature. Then the $ZrO_2$ nanoparticle was obtained via controlled calcination process using muffle furnace for 3hrs at 500 ºC (method A).

In Co-precipitation method, 3.3 *m*mol KOH was dissolved in 36 ml distilled water under stirring. Then 3 mmol the template, hexamethylenetetramine, was added to the solution. Zirconium chloride (3 mmol) was added to the mixture. The mixture was refluxed for 4 h in 110 ºC. $ZrO_2$ was obtained by centrifugation and drying of precipitate at room temperature. Then the $ZrO_2$ nanoparticle was obtained via controlled calcination process using muffle furnace for 3hrs at 600 ºC (method B).

The effect of amount of $ZrO_2$ nanoparticle as photocatalyst on the efficiency of photocatalytic decomposition of CIP in aqueous solution was investigated. The degradation experiments were carried out in the 500 mL of 15 ppm CIP. Before irradiation, the suspensions were magnetically stirred in the dark for over 30 min to ensure adsorption equilibrium of CIP with the photocatalysts, and then exposed to UV light. The pH of solutions was adjusted in the range 5–9 after the addition of the catalyst. The maximum removal efficiency was obtained at pH 5.5. The concentration of CIP was determined by measuring the absorption intensity at its maximum absorbance wavelength at 270 nm and 320 nm with a UV–vis spectrophotometer.

**RESULTS AND DISCUSSION**

Fig. 1 provides a comparison of typical XRD patterns of products obtained from green chemistry (a) and co-precipitation (b) methods in an aqueous solution. In Fig. 1a, all reflection peaks of XRD pattern of $ZrO_2$ nanoparticles are indexed well to monoclinic phase of $ZrO_2$.The peaks located at 24.58 °, 31.57°, 34.30°, 49.35°, and 59.89 correspond to crystal planes of (110), (111), (002), (022), and (131) monoclinic crystalline structure of $ZrO_2$ (JCPDS-37-1484). The XRD pattern of the sample B is shown in Figure 1b. The peaks at 30.2°, 50.2° and 60.2° corresponding to the characteristic diffraction planes (1 1 1), (3 0 2) and (3 1 1) of $ZrO_2$ in tetragonal phase, which is in good agreement with reported data (JCPDS No.81-1544) . From XRD data, the crystallite diameter (Dc) of $ZrO_2$ nanoparticles were calculated by using the Scherer Eq. to be 28 and 15 nm for samples A and B, respectively. Figs. 2a, b show the EDX spectra of sample A, B. The EDX spectra revealed that the synthesized products are well consistent with the XRD results.

Fig. 3a-3d presents the corresponding FeSEM and TEM images, which illustrate the size and shape of the extracted $ZrO_2$ particles. For method A and B, the $ZrO_2$ nanoparticles appear to be in the range of 29-32 and 14-18 nm, respectively. It seems that this methods lead to finer particle size in comparison with other processing technique such as mechanical alloying.

The Ft-IR spectrum of t-$ZrO_2$ NPs is shown in Fig. 4b. Peaks provided at 3412 cm$^{-1}$, 1620 and 492.73 cm$^{-1}$ due to OH stretching, OH bending and Zr-O band, respectively. The characteristic peak of m-ZrO2 is seen at 764 cm$^{-1}$ (Fig. 4a). A higher amount of surface hydroxyl groups over
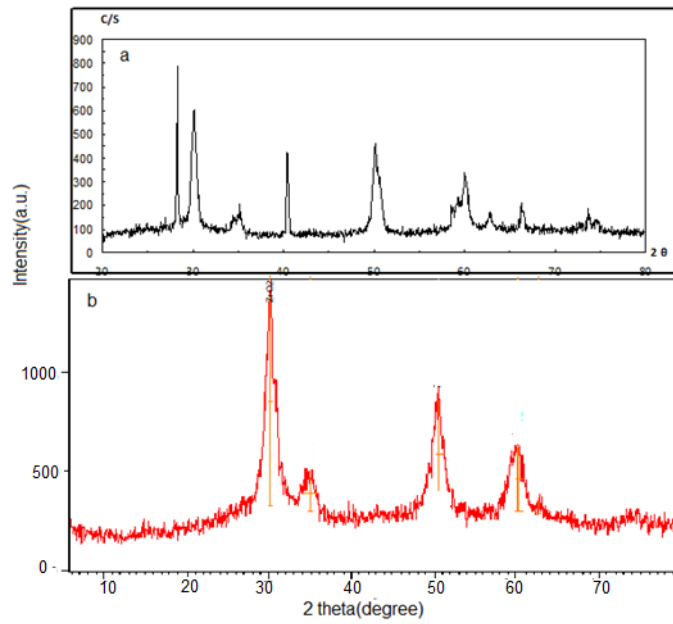
Fig. 1. XRD pattern and EDX spectra of the synthesized ZrO$_2$ nanoparticles with a) method A, b) method B.
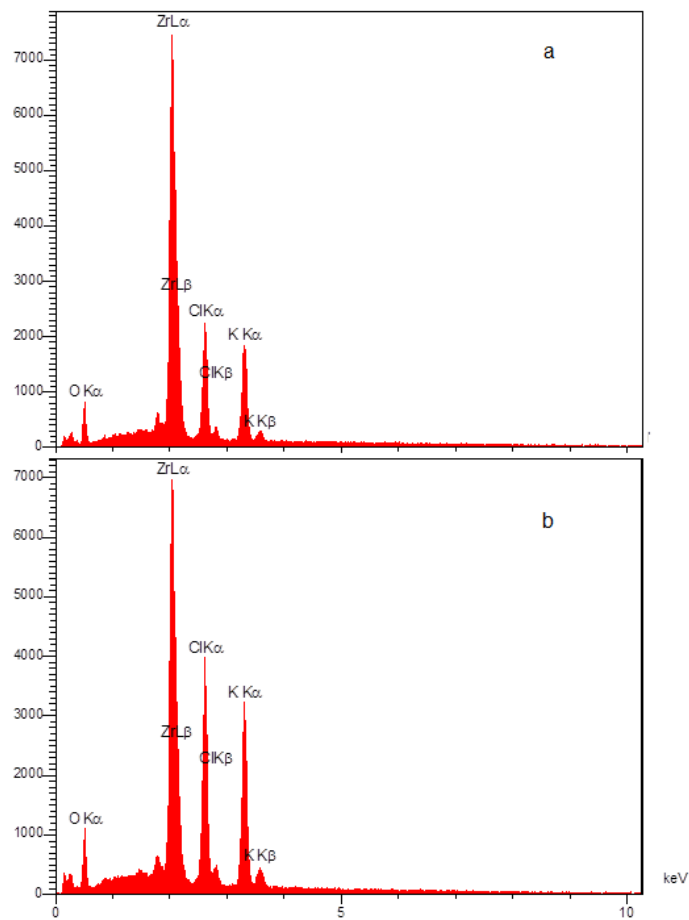


Fig. 2. EDX spectra of different samples a) method A, b) method B.
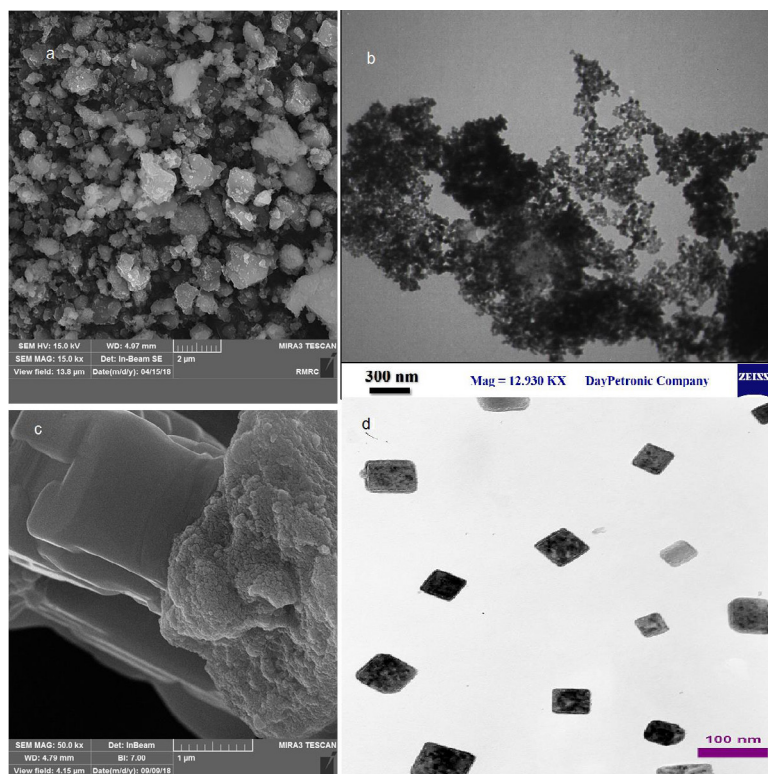
Fig. 3. FeSEM and TEM images of the synthesized ZrO$_2$ nanoparticles with method:   a, b) method B, c, d) method A.
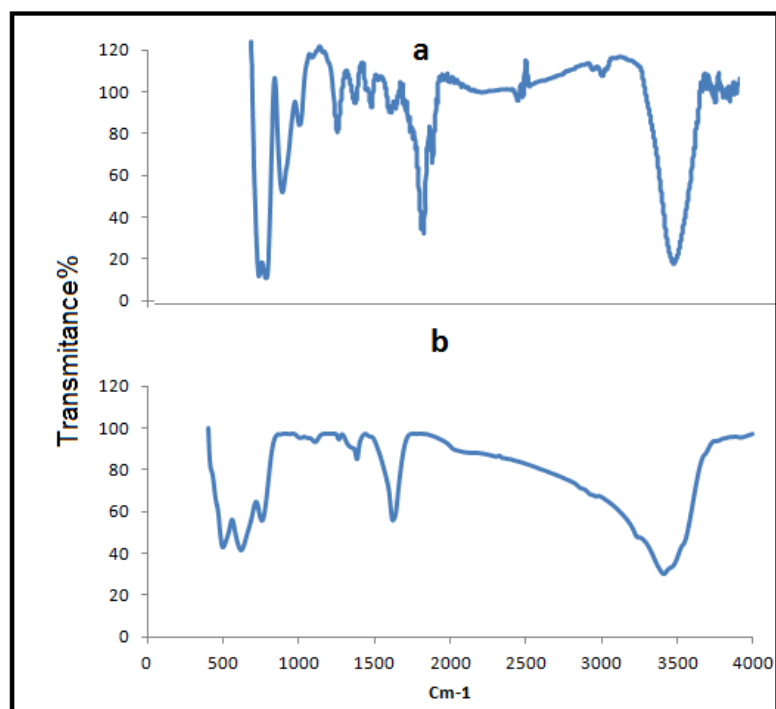


Fig. 4. FT-IR spectra of synthesized ZrO$_2$ nanoparticles with method: a) method A, b)  method B.
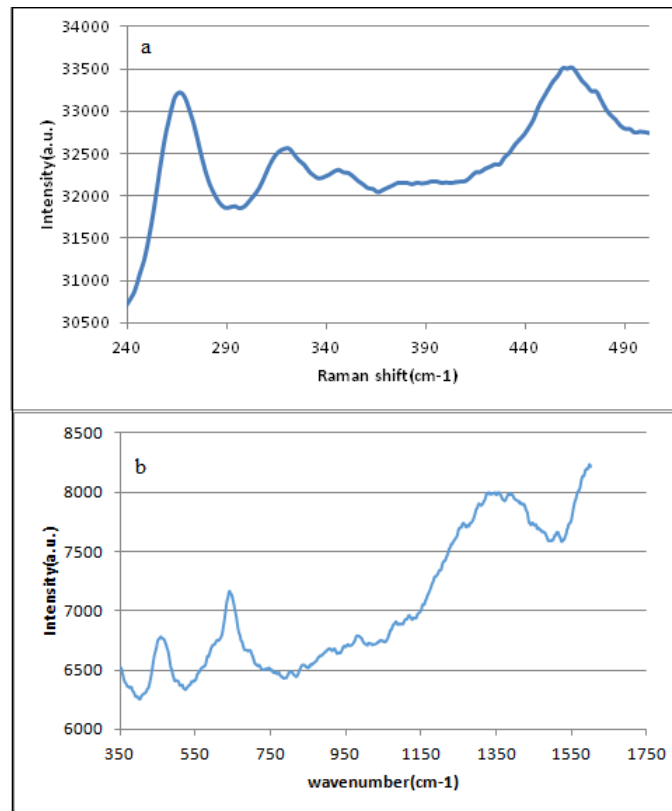
Fig. 5. Raman spectra of ZrO$_2$ nanoparticles with method:  a) method A, b) method B.

ZrO$_2$ showed high potential in the photocatalytic activity.

Raman spectroscopy is recognized as a powerful tool for identifying different polymorphs of metal oxides [25]. According to group theory, active modes are 18 (9Ag+9Bg) and 6 (1A1g+2B1g+3Eg) for monoclinic (m-ZrO$_2$) and tetragonal (t-ZrO$_2$), respectively [26]. Raman active lattice phonons were expected in spectral region 100-550 cm$^{-1}$ for Zirconia with low phonon energy, The Raman bands at 147 and 260 cm$^{-1}$ (Eg and B1g) confirms the presence of tetragonal phase [27] [Fig. 5a]. The Raman spectra shown in Fig. 5b have peaks at, 476 and 590 cm$^{-1}$, which are all attributed to the monoclinic phase of ZrO$_2$ [28-30].

In general, pure ZrO$_2$ shows various emission of a broad band that is dependent on preparation methods and wavelength excitation [31].  Band gap energy of the loaded samples was estimated by Kubelka–Munk function using Eq )1):

$$\alpha = \frac{A(E_g - h\nu)^n}{h\nu} \tag{1}$$

Where E$_g$ is the band gap of the proposed semiconductor (eV), A is constant and n is equal to 1/2 for direct transition, and $_{\iota}\alpha$ is the absorption coefficient defined by the Beer–Lambert's law. The plot of $(\alpha h\nu)^2$ Vs h$\nu$ of ZrO$_2$ is shown in Fig. 6a, b. According to Fig. 6 a, b, band gaps of method A and B are calculated 2.8 and 3.9 eV, respectively. The size reduction in the nanoparticle can cause the change in optical band gap of metal oxides that affects defect centers and mechanical stress.

Fig. 7a, b shows the optical absorption spectra of CIP using ZrO$_2$ nanoparticles as a photocatalyst under UV light radiation. The absorption spectrum of the drug shows two strong peaks at 277 nm and 320 nm. As seen in the figure, the decomposition of the drug increasess with increasing irradiation time. ZrO$_2$ surface is acidic and the rate of degradation increases under acidic conditions. The effect of pH on CIP adsorption on the surface of zirconia has been investigated in the range of 5 to 9. The optimum pH is 5.5. For investigating of the effect of ZrO$_2$ concentration on photocatalytic efficiency, a set of experiments was performed
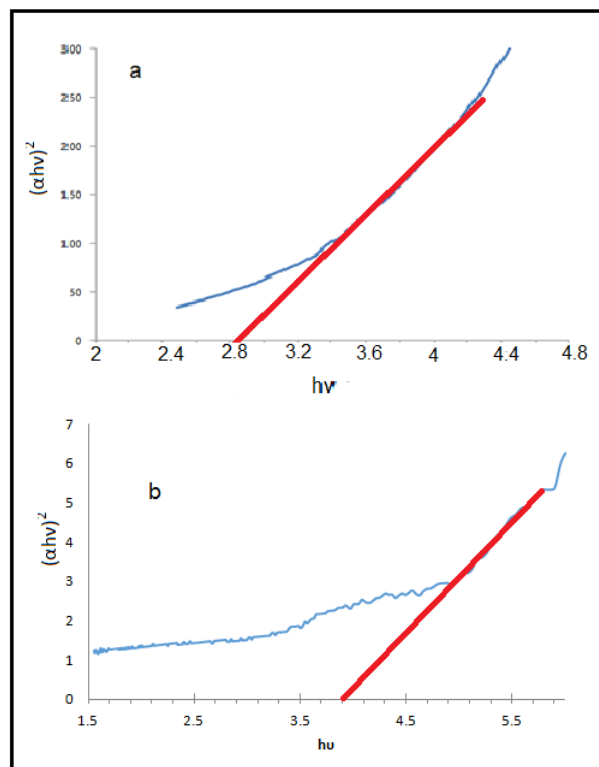
Fig. 6. Plot of transferred Kubelka–Munk versus energy of the light absorbed of the ZrO$_2$ nanoparticles with method: a) method A, b) method B.
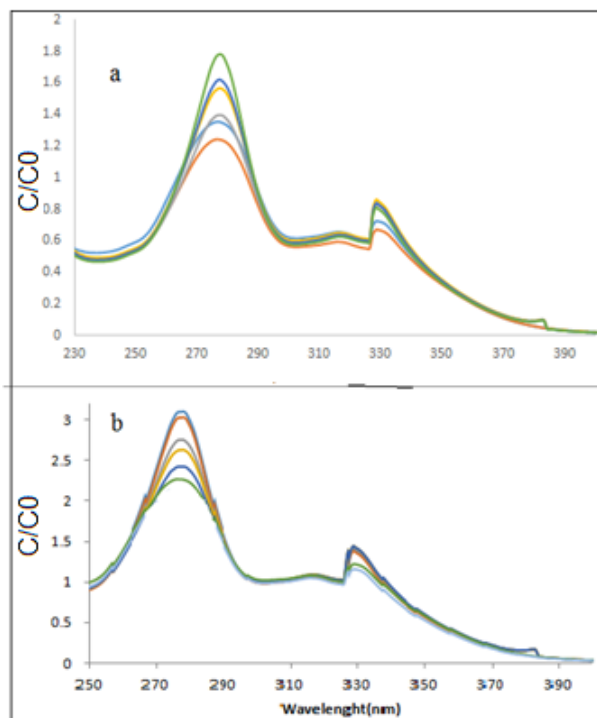


Fig. 7. Decrease in the UV–vis absorption of CIP in pH = 5.5 at its λmax during the photodegradation with irradiation time 0-90 min with irradiation time 0-15 min a) method B, b) method A.

with different concentrations of $ZrO_2$ in a range from 0.2–1.1 g/L. The results showed that the optimum concentration of $ZrO_2$ catalyst is 1.0 g/L. The photocatalytic activity of $m$-$ZrO_2$ and $t$-$ZrO_2$ nano oxides reaches 50% (Fig. 7a) and 36% (Fig. 7b) after 15 min, respectively.

**CONCLUSIONS**

In summary, the results obtained proved that nano $ZrO_2$ could be successfully prepared via reflux and using two templates. We present a new rout for synthesis of pure tetragonal and monoclinic $ZrO_2$ with high crystalinity, using a rapid, simple and cost-effective chemical method. The good quality of zirconia shows that our method is better than previous studies. In a study, researchers shown that the pure tetragonal crystalline phase was characterized by an average 13 nm crystallite size. For a larger crystallite size (65.2 nm), monoclinic $ZrO_2$ appears crystallite size [32]. Synthesis method, precursor and template type affect physical properties such as morphology of nanoparticles. The presence of antioxidants (either polyphenols or ascorbic acid), allow coffee, to reduce metal ions to form metal nanoparticles. For this reason monoclinic $ZrO_2$ were appearance simultaneous with the 28 nm crystallite size. Particle size varies depending on the method of preparation. Internal stresses related to the mechanical balance between the surface and the volume state change the wavenumbers. The photocatalytic activity is mainly ascribed due to the high crystallinity, number of oxygen vacancies, surface area and pore volume.

**Conflict of interest**

The authors declare that there is no conflict of interest.

**References**

[1] Okabe E., Ishihara Y., Kikuchi T., Izawa A., Kobayashi S., Goto H., Kamiya Y., Sasaki K., Ban S., Noguchi T., (2016), Adhesion properties of human oral epithelial-derived cells to zirconia. *Clin. Implant Dent. Relat. Res*. 18: 906–916.

[2] Xuhui W., Jinxian Z., (2020), Effects of surface acid–base properties of $ZrO_2$ on the direct synthesis of DMC from $CO_2$ and methanol: A combined DFT and experimental study. *Chem. Eng. Sci*. 229: 116018.

[3] Morozova L. V., Kalinina M. V., Koval'ko N. Y., Arsent'ev M. Y., Shilova O. A., (2014), Preparation of zirconia based nanoceramics with a high degree of tetragonality. *Glass. Phys. Chem*. 40: 352–355.

[4] Assi N., Mehrdad Sharif A., Manuchehri Naeini Q. S., (2014), Synthesis, characterization and investigation photocatalytic degradation of Nitro Phenol with nano ZnO and $ZrO_2$. *Int. J. Nano Dimens.* 5: 387-391.

[5] Wilk G. D., Wallace R. M., Anthony J. M., (2001), High-κ gate dielectrics: Current status and materials properties considerations. *J. Appl. Phys*. 89: 5243-5249.

[6] Bill G. X., Zhang Damian E., Myers Gordon G., Wallace Milan Brandt Peter F., Choong M., (2016), Bioactive coatings for orthopaedic implants—recent trends in development of implant coatings. *Int. J.Mol. Sci.* 15: 11878-921.

[7] Shin J. H., Chao C., Huang H., Prinz F. B., (2007), Atomic layer deposition of yttria-stabilized zirconia for solid oxide fuel cells. *Chem. Mater*. 19: 3850-3861.

[8] Leo´n C., Lucia M. L., (1997), Correlated ion hopping in single-crystal yttria-stabilized zirconia. *J. Phys. ReV. B.* 55: 882-887.

[9] Garvie R. C., Hannink R. H., Pascoe R. T., (1975), Influence of nanocrystalline $ZrO_2$ additives on the fracture toughness and hardness of spark plasma activated sintered $WC/ZrO_2$ nanocomposites obtained by mechanical mixing method. *Nature.* 258: 703-709.

[10] Stichert W., Schuth F., Kuba S., Knozinger H., (2001), Monoclinic and tetragonal high surface area sulfated zirconias in butane isomerization: CO adsorption and catalytic results *J. Catal*. 198: 277–285.

[11] Jung K. T., Bell A. T., (2000), The effects of synthesis and pretreatment conditions on the bulk structure and surface properties of zirconia. *J. Mol. Catal. A*. 163: 27–42.

[12] Djurado E., Meunier E. J., (1998), Synthesis of doped and undoped nanopowders of tetragonal polycrystalline zirconia (TPZ) by spray-pyrolysis. *Solid. State. Chem*. 141: 191–198.

[13] Shukla S., Vanfleet R., (2003), Sol-Gel synthesis and phase evolution behavior of sterically stabilized nanocrystalline zirconia. *J. Sol-Gel Sci. Technol*. 27: 119–136.

[14] Shukla S., Seal S., (2005), Mechanisms of room temperature metastable tetragonal phase stabilization in zirconia. *Int. Mater. ReV*. 50: 45–64.

[15] Shukla S., Seal S., (2004), Thermodynamic tetragonal phase stability in Sol–Gel derived nanodomains of pure zirconia. *J. Phys. Chem. B*. 108: 3395–3399.

[16] Shukla S., Seal S., Vij R., Bandyopadhyay S., Rahman Z., (2002), Effect of nanocrystallite morphology on the metastable tetragonal phase stabilization in zirconia. *Nano Lett.* 2: 989–993.

[17] Jiahe L., Zhaoxiang D**.,** (2003), Photoluminescence of tetragonal $ZrO_2$ nanoparticles synthesized by microwave irradiation. *Inorg. Chem.* 41: 3602-3604**.**

[18] Joo J., Yu T., Kim T. Y. W., Park H. M., Wu F., Zhang J., Hyeon T., (2003), Multigram scale synthesis and characterization of monodisperse tetragonal zirconia nanocrystals. *J. Am. Chem. Soc.* 125: 6553–6557.

[19] Sun Q., Zhang Y., Deng J., Chen S., Wu D., (1997), A novel preparation process for thermally stable ultrafine tetragonal zirconia aerogel. *Appl. Catal. A*. 152: L165-L171.

[20] Clifford M. N., (1987), Chemical and physical aspects of green coffee and coffee products. In: Coffee: botany, biochemistry and production of beans and beverage. *Clifford MN; Willson KC (eds)*, pp. 457. Chroom Helm,

Sydney, Australia.

[21] Ou C., Yang C., Lin S., (2011), Selective photo-degradation of Rhodamine B over zirconia incorporated titania nanoparticles: A quantitative approach. *Catal. Sci. Technol.* 1: 295–307.

[22] Wang X., Zhang L., Lin H., Nong Q., Wu Y., He Y., (2014), Synthesis and characterization of a $ZrO_2/g-C_3N_4$ composite with enhanced visible-light photoactivity for rhodamine degradation. *RSC Adv.* 4: 40029-40036.

[23] Ma S., Maeda K., Domen K., (2012), Modification of TaON with $ZrO_2$ to improve photocatalytic hydrogen evolution activity under visible light: influence of preparation conditions on activity. *Catal. Sci. Technol*. 2: 818–823.

[24] Tai C. Y., Hsiao B. Y., (2005), Characterization of zirconia powder synthesized via reverse micro emulsion precipitation. *Chem. Eng. Commun*. 192: 1525-1540.

[25] Singh K. A., Pathak L. C., Roy S. K., (2007), Effect of citric acid on the synthesis of nanocrystalline yttria stabilized zirconia powders by nitrate-citrate process. *Ceram. Int*. 33: 1463–1468.

[26] Reena D., Anjali M., Akrati V., Prasad R., Bartwal K. S., (2011), Microwave assisted sol–gel synthesis of tetragonal zirconia nanoparticles. *J. Alloy. Comp.* 509: 6848–6851.

[27] Angeles-Rosas M., Camacho-López M. A., Ruiz-Trejo E., (2010), Structure, conductivity and luminescence of 8 mol% scandia-doped zirconia prepared by sol–gel. *Solid State Ion*. 181: 1349–1354.

[28] Ling X., Li S., Zhou M., Liu X., Zhao Y., Shao J., Fan Z., (2009), Annealing effect on the laser-induced damage resistance of $ZrO_2$ films in vacuum. *Appl. Opt*. 48: 5459–5463.

[29] Kumari L., Du G. H., Li W.Z., Vennila R. S., Saxena S. K., Wang D.Z., (2009), Synthesis, microstructure and optical characterization of zirconium oxide nanostructures. *Ceram. Int*. 35: 2401–2408.

[30] Kumari L., Li W. Z., Wang D. Z., (2008), Monoclinic zirconium oxide nanostructures synthesized by a hydrothermal route. *Nanotechnol.* 19: 195602-195608.

[31] Smits K., Grigorjeva L., Millers D., Sarakovskis A., Grabis J., Lojkowski W.,

(2011), Intrinsic defect related luminescence in $ZrO_2$. *J. Lumin*. 131: 2058-2062.

[32] Djurado E., Bouvier P., Lucazeau G., (2000), Crystallite size effect on the tetragonal-monoclinic transition of undoped nanocrystalline zirconia studied by XRD and Raman spectrometry. *J. Solid State Chem.* 149: 399-407.